ELSEVIER

Journal of Nuclear Materials 241–243 (1997) 167–181

journal of nuclear materials

A review on impurity transport in divertors

K. Shimizu *, T. Takizuka, A. Sakasai

Japan Atomic Energy Research Institute, Naka Fusion Research Establishment, Naka-machi, Naka-gun, Ibaraki-ken 311-01, Japan

Abstract

Power exhaust is one of the most crucial requirements for future fusion reactors, like ITER. It is widely recognized that impurity injection is needed to significantly reduce the heat load to the divertor plates. By controlled injection of light impurities, the compatibility of high confinement core plasma with strong radiative divertor has been successfully demonstrated in many tokamaks. However, the core impurity contamination was high ($Z_{eff} \sim 3$) compared to the value required for ITER ($Z_{eff} < 1.6$). Therefore, a scheme for impurity retention in the divertor region should be established for fusion research. This paper reviews the recent progress in experiments and simulations which have been made for the purpose of understanding impurity transport in divertors. The issues contained in the paper are impurity generation, shielding and cross field diffusion. As for the impurity generation, chemical sputtering and wall source are discussed with emphasis on the characteristics of their transport and shielding. Impurity control with plasma flow induced by gas puffing and divertor pumping, and adequately designed divertor geometry is also presented.

Keywords: Fluid simulation; Monte Carlo simulation; Impurity transport; Impurity source; Physical erosion; Chemical erosion

1. Introduction

Impurity control is one of the most crucial requirements for future fusion reactors, like ITER. Excessive impurity content in the main plasma degrades energy confinement due to impurity radiation and reduces the fusion power due to fuel dilution. For this reason, in the main plasma, low impurity concentration must be maintained. On the other hand, impurity radiation at the plasma edge and in the divertor region is very effective in reducing the heat load onto the divertor plates. In ITER, 100 MW must be radiated in the divertor region [1]. Therefore, a scheme for impurity retention in the divertor region should be established for fusion research. This paper reviews the recent progress in experiments and simulations which have been carried out for the purpose of impurity control.

By means of strong gas puffing and introduction of light impurities, the compatibility of high confinement core plasma (H-mode) with strong radiative divertor has been demonstrated in DIII-D [2], JET [3] and Alcator C-mod [4]. A completely detached divertor has been attained in ASDEX-Upgrade H-mode [5]. In negative shear discharges in JT-60U, the detached divertor has been recently achieved for 1.8 s by neon gas puffing with the internal transport barrier sustained [6]. Impurity injection plays an essential role in achieving of high confinement core plasmas with the radiative divertor. However, applying the impurity injection scenario to ITER would confront a serious problem, i.e., high impurity concentration in the core plasma. Fig. 1 shows a typical discharge with detached radiative divertor in JET [7]. The divertor radiation was enhanced by deuterium gas puffing and introduction of nitrogen impurities. The divertor plasma was detached fully from the target plate after $t = 16.6$ s. At this time the radiated power fraction rose to about 85% of the input power. This fraction is sufficient for heat exhaust in ITER. The achieved H-factor was 1.5, which is barely sufficient for ITER confinement. However, the core impurity contamination was high ($Z_{eff} \sim 3$) compared to the value required for ITER ($Z_{eff} < 1.6$) [1].

To achieve sufficiently low core impurity content and sufficiently high divertor impurity density simultaneously, a scheme for impurity retention in the divertor region

* Corresponding author. Tel.: +81-29 270 7431; fax: +81-29 270 7319; e-mail: kshimizu@naka.jaeri.go.jp.

PII S0022-3115(96)00503-X

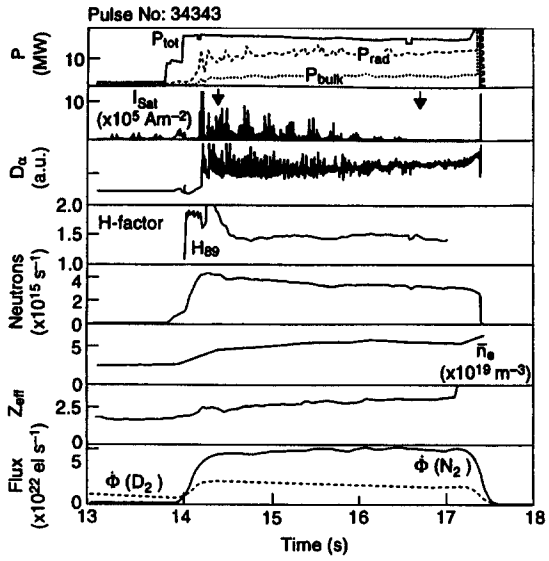

Fig. 1. Detached radiative divertor plasma achieved by nitrogen puff. Time evolution of total input power (P_{tot}), divertor radiation (P_{rad}), bulk radiation (P_{bulk}), ion saturation current at the targets (I_{sat}), D_α emission, confinement enhancement factor relative to the ITER89-P L-mode scaling (H-factor), neutron yield, line averaged plasma density ($\bar{n}_e$), effective charge (Z_{eff}), deuterium puff rate ($\dot{\Phi}$ (D_2)), and nitrogen puff rate ($\dot{\Phi}$ (N_2)). The ion saturation current indicated that the divertor plasma was detached fully from the target plate after $t = 16.6$ s (taken from JET experiments [7]).

should be established. Understanding of impurity transport is indispensable for this achievement. Impurity transport involves various physical processes, as shown in Fig. 2. The issues to be addressed in impurity study are source, shielding and cross-field diffusion.

This review paper is organized as follows. In Section 2, representative simulation codes are introduced and the assumptions widely used in fluid codes are discussed. Impurity production is reviewed in Section 3, and shielding and cross-field diffusion are discussed in Section 4. Impurity control by gas puffing and divertor pumping, and optimization of divertor geometry for impurity shielding

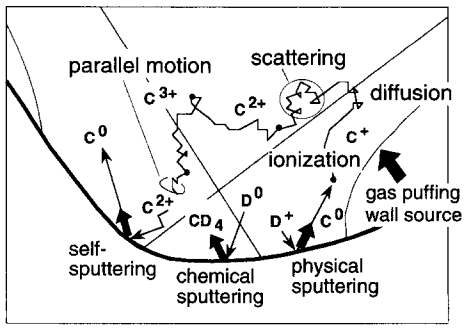

Fig. 2. Physical processes to be addressed in impurity study.

are presented in Section 5, and conclusions are summarized in Section 6.

2. Simulation code

Both the impurity transport and the SOL plasma transport are strongly coupled with each other through the force acting on impurity ions and radiation loss. This interaction determines the impurity density profile, which is highly asymmetric in the poloidal plane. Since in most of the diagnostics for impurity study, such as spectrometer and bolometer, line-integrated quantities are measured, some information on impurity distribution is missing in these measurements. Flow velocity and temperature in the SOL strongly influences impurity transport, but there are few measurements of such plasma parameter so far. Hence 'missing profile data' on both the background plasma parameters and the impurity distribution must be supplemented by simulation code.

However, the diagnostics has been developed remarkably in the last two years: Measurements of flow velocity with Mach probe on TdeV [8] and Alcator C-mod [9], and 2D measurements of electron temperature and density with Thomson scattering system in the divertor on DIII-D [10] has been made. In many tokamaks, 2D radiation profile has been constructed from multi-channel bolometer signals by using a tomographic techniques [2,4,11,12], as well as 2D emission profiles of impurities from spectroscopic measurement [13,14]. Furthermore, DIII-D has recently developed the capability to produce 2D distribution of impurities in the poloidal plane with an extensive set of divertor measurements [15]. Such 2D profiles will provide us useful information to understand impurity transport; nevertheless, data obtained with a tomographic algorithm contains some uncertainty and are limited for special charge state. Not all plasma parameters are directly measured. Therefore, simulation is still necessary for interpretation of the line integrated quantities or for the 'missing profile data'. In addition, simulation analysis make it possible to clarify the complicated interactions between the plasma and impurities. Thus simulation analysis plays an essential role in understanding impurity behavior in the divertor.

Simulation codes are classified into fluid codes and Monte Carlo codes. They are summarized in a review paper by Stangeby [16]. An early analysis was performed on ASDEX by a 1D parallel flow code [17,18], and then a number of 2D multi-fluid divertor codes have been developed, e.g., B2 [19], EDgE2D [20], UEDgE [21], DDIC [22] and UEDA [23]. In these codes, impurity transport is solved simultaneously with background plasma transport under realistic divertor configurations. The recent analysis results with such fluid codes are described in a review paper by Loarte [24]. A Monte Carlo impurity transport code was pioneered by Sengoku et al. [25]. It has been

followed by Brooks, who has developed REDEP [26] and ZTRANS [27]. Recently elaborate Monte Carlo codes have been developed for the interpretation of impurity behavior in the divertor, e.g., DIVIMP [28], IMPMC [29] and MCI [30]. In Monte Carlo codes, the background plasma parameters are frequently specified with interpretative simple divertor codes named 'Onion-Skin model' [28,31–33], in order to take full advantage of experimental data available. In the Onion-Skin model, fluid equations along the field line in each flux tube are solved numerically with experimental boundary conditions at the plates, (i.e., Langmuir probe data). Since recent improvements in 2D divertor codes can satisfactorily reproduce most of experimental measurements in the SOL, the profiles calculated with the UEDGE code are used as the background plasma in the MCI code. The DIVIMP code can also use background plasma parameters calculated with the EDGE2D code.

Though Monte Carlo codes have a disadvantage of long computational time, they have two advantages for impurity modelling. First, one can take into account the parallel motion and various collisional effects, such as ionization, recombination and Coulomb scattering with the background particles, correctly and simultaneously. Second, one can model impurity generation and interactions between impurities and walls in a realistic geometry. In these respects, Monte Carlo models are superior to fluid models, in which high collisionality are implicitly assumed. This assumption in a fluid model is not always appropriate, especially for impurities with low charge states, whose ionization time or transit time for the parallel motion is shorter than the collision time with the plasma.

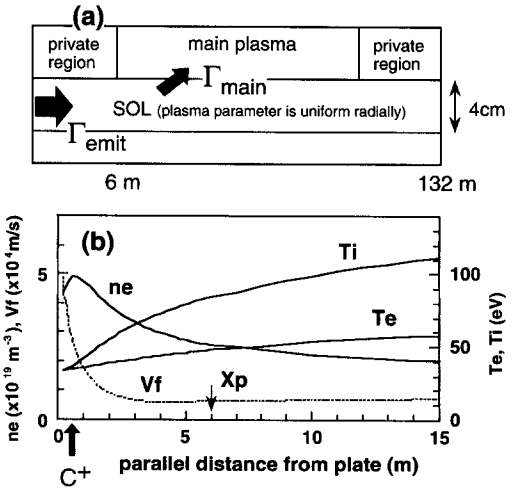

Fig. 3. (a) Geometry used in the 1D-Monte Carlo simulations. The pirch of the field lines is taken as constant, $B_\theta / B = 0.025$. (b) Plasma parameters along the field lines. The X-point is located at 6 m from the target plate. The carbon impurities are assumed to be ionized at the point shown by an arrow, correspond to $\lambda_{ion} = 1.4$ cm.

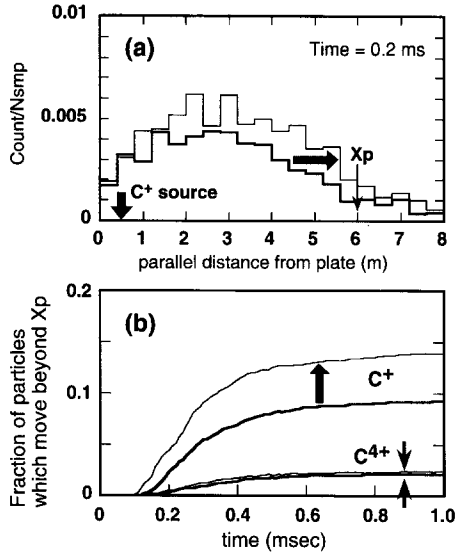

Fig. 4. (a) Calculated impurity density along the field lines at $t = 0.2$ ms. Bold line represents the density calculated with the normal model, thin line represents the density calculated with the assumption that C^+ ions are thermalized instantaneously at $t = 0$. (b) Time evolution of fraction of particles which move beyond the X-point. The ionization state is taken to be fixed throughout each calculation for C^+ and C^{4+} ions.

Using a 1D-Monte Carlo code, therefore, we check two assumptions widely used in fluid codes: Instantaneous thermalization of impurity ions ($T_{imp} = T_i$) and simplified evaluation of self-sputtering outflux. The physical processes included in the code are the same as those of the IMPMC code [29]. A simple impurity generation model is employed instead of the Thompson model [34], which determines the distributions of angle and velocity of sputtered neutrals. The carbon impurities are sputtered at 10 eV and in the normal direction to the plate. They are assumed to be ionized at some specified distance from the plate ($\lambda_{ion} = 1.4$ cm). The geometry used in the following simulations is illustrated in Fig. 3(a). The width of SOL is 4 cm and the plasma parameters vary along magnetic field lines as shown in Fig. 3(b). For simplicity, the divertor plasma is assumed to be radially uniform. The electron density at the plate is $n_{ed} = 4 \times 10^{19}$ m^{-3} and the electron and ion temperatures are $T_{ed} = T_{id} = 30$ eV. These parameters correspond to divertor plasmas at intermediate density ranges in JT-60U and JET. Twenty thousand test particles are placed at the point shown by an arrow, and they are followed until they hit the plate or wall or enter the main plasma. The penetration probability (P) is defined as the ratio of the number of particles entering the main plasma to the number of the total test particles. Fig. 4(a) shows the calculated impurity density along the field lines at 0.2 ms. The bold line represents the density calculated with the normal model, in which the thermalization process is

simulated by the Monte Carlo method. On the other hand, the thin line represents the density calculated with the assumption that C^+ ions are thermalized instantaneously at $t = 0$. The density profile is spread towards the upstream in case of the instantaneous thermalization. As a result, the probability of penetration into the main plasma is enhanced from 2.2% to 3.1%. The applicability of this assumption is examined separately for various ionization states. The ionization state is taken to be fixed throughout each calculation. Fig. 4(b) shows the time evolution of the fraction of particles which move beyond the X-point for C^+ and C^{4+}. The result indicates that the assumption of $T_{imp} = T_i$ can not be applied for C^+ ions, while it is a good assumption for C^{4+} ions due to their short thermalization time (the collision frequency $\propto Z^2$), as expected.

In the fluid model, self-sputtering outflux is evaluated as follows. The impurities are originally sputtered from the plate by deuterium physical sputtering. Its outflux is evaluated by $\Gamma_0 = Y_D n_D C_S$, where Y_D is the physical sputtering yield by deuterium ions [35], and C_S is the sound speed. The sputtered neutrals are ionized and most of them return to the plate by the friction force with background ions. These impurities cause sputtering with the initial self-sputtered flux of $\Gamma_0 f Y_C$, where f is the fraction of sputtered impurities returning to the plate and $Y_C(E_C)$ is the sputtering yield. The dependence of Y_C on the incident energy E_C is given in Ref. [35]. The incident energy of impurity ions is assumed as follows:

$$E_0^{simple} = \tfrac{5}{2}T_i + \tfrac{1}{2}m_I C_S^2 + eZ\phi_S. \quad (1)$$

The second term in RHS means that impurity ions are assumed to acquire a flow velocity equal to that of the background plasma due to the friction force. This physical picture is incorrect for low charge state ions, as shown below. The third term represents the acceleration due to the sheath potential $\phi_S \approx 3T_{ed}$. Usually, f is taken to be 1 in the simple estimation, although $f < 1$ in the real situation. Self-sputtered impurities of the first generation also return to the plate and cause sputtering with the second self-sputtered flux of $\Gamma_0 f^2 Y_C^2$, and so on. Thus the net outflux of self-sputtering is approximately evaluated by

$$\Gamma_{self} = \Gamma_0 f Y_C / (1 - f Y_C). \quad (2)$$

On the other hand, the self-sputtering process can be treated self-consistently in the Monte Carlo code where the impurity ion dynamics are taken into account. The difference in the incident energy and the outflux between the simple evaluation and Monte Carlo calculation are listed in Table 1 for the same plasma parameters as in Fig. 3. The incident energy is expressed in the unit of eV. For the case that neutral particles are ionized close to the plate ($\lambda_{ion} = 0.4$ cm), the difference becomes large. It is found that the incident energy of C^+ and C^{2+} is overestimated in the fluid code, and that this leads to overestimation of the total self sputtering outflux by a factor of 1.2 or 1.7, depending on the ionization position. Furthermore, these factors are enhanced when the angular dependence of incident ions onto the plate and the fraction of $f < 1$ are taken into account. In the low density divertor plasma, the simple estimation evaluates a flux 5–6 times higher than that calculated with a Monte Carlo code [29]. It should be noted that in the high density plasma, C^{2+} ions become dominant in ions returning to the plate, which can hardly be treated by a fluid model with accuracy. These results indicate that the Monte Carlo approach is indispensable for an accurate analysis of self-sputtering.

Table 1
Comparison of averaged incident energy (E_0) of ions hitting the target plate and resultant outflux (Γ) due to self-sputtering between the simple evaluation used in fluid codes and Monte Carlo calculation

	C^+	C^{2+}	C^{3+}	C^{4+}
(a) $\lambda_{ion} = 1.4$ cm				
Fraction	< 0.1%	12.2%	66.0%	21.8%
$E_0(F)/E_0(MC)$	387/232	484/338	586/473	687/589
$\Gamma(F)/\Gamma(MC)$	1.9	1.4	1.2	1.1
(b) $\lambda_{ion} = 0.4$ cm				
Fraction	3.9%	47.3%	44.6%	4.1%
$E_0(F)/E_0(MC)$	387/118	484/273	586/439	687/578
$\Gamma(F)/\Gamma(MC)$	5.2	1.8	1.3	1.1

3. Impurity production

In large and medium-sized tokamaks, high plasma performance has been achieved by application of low Z materials, such as carbon and beryllium to the divertor plates and/or walls. In addition, various techniques of wall conditioning, e.g., Taylor-type discharge cleaning (TDC), glow discharge cleaning (GDC) and boronization, have been extensively developed to significantly reduce oxygen impurities [36]. As a result, carbon, which is the material of the divertor plates, has become the major impurity in most of the present tokamaks. Therefore, the focus of this section is on the carbon production mechanism. Various production mechanisms of light impurities are described comprehensively in recent review papers by Pitcher and Stangeby [37], and by Davis and Haasz [38] and in the textbook edited by Hofer and Roth [39]. In this section, we discuss chemical sputtering and wall source, with emphasis on their characteristics of transport and shielding.

3.1. Chemical sputtering

In the JT-60U tokamak, the carbon outflux from the divertor plates was estimated according to the expressions of Eqs. (1) and (2) using T_e and n_e measured with Langmuir probes. From the comparison with the spectro-

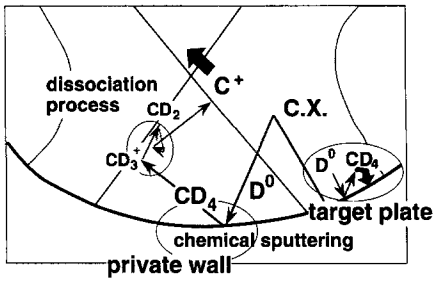

Fig. 5. Mechanism to explain existence of C^+ ions near the X-point.

scopic measurement of C II line, it was concluded that in the neutral beam heated plasmas at low and intermediate densities, carbon impurities are generated mainly by the physical sputtering by deuterium ions and self-sputtering [40,41]. This conclusion has been reconfirmed by the simulation analysis with the IMPMC code [29].

In discharges with strong gas-puffing, however, a change in the C II line radiation profile was observed [42]. The profile showed two peaks at the separatrix strike points in a low density phase. The peaks started to decrease with increasing plasma density due to gas-puffing, while the intensity between the strike points started to increase. The peaks finally moved away from the strike points to the neighborhood of the X-point, followed by the occurrence of a MARFE. The intensity measured in the private region indicates that C^+ ions exist near the X-point even in the attached plasma with temperature above 10 eV. However, a simple consideration for the penetration length shows that carbon released from the divertor plates are ionized to C^{3+} or C^{4+} ions before they reach near the X-point. The simulation calculated with the IMPMC code also showed that the contribution of physical sputtering to the C II line radiation was negligibly small near the X-point (see Fig. 6).

Then how can C^+ ions approach the X-point? Fig. 5 illustrates this mechanism [43]. In high density and low temperature divertor plasmas, the charge exchange process becomes dominant in the neutral transport and the influx of neutrals to the wall increases with plasma density. The incident energy of neutral particles is small because of no acceleration due to sheath potential. The mean incident energy is about 20 eV on the divertor plates and 50 eV on the private wall [43], which is less than the threshold energy for physical sputtering. On the other hand, chemical sputtering has no threshold energy and the yield is fairly high at low incident energy (typically ~ 0.05 at the plate temperature < 1000°C) [35,44]. The neutral particles hitting the divertor plate or wall cause chemical sputtering. Methane sputtered from the private wall is dissociated or ionized in the private region where the cold and thin plasma exists near the separatrix. Carbon originating from methane easily enters the main plasma since shielding is less effective there. As a result, the C II line intensity near the X-point increases.

On the basis of this physical mechanism, the simulation analysis has been carried out with IMPMC, in which the dissociation process of methane and the dynamics of dissociation products, such as CD_4^+, CD_3 and CD_3^+, are included. The dissociation time of methane to C^+ ion is much longer than the ionization time of carbon atom by a factor of 10, in a uniform plasma with $n_e = 1 \times 10^{19}$ m^{-3}, $T_e = 20$ eV [45]. However, the penetration length of C^+ ions dissociated from methane is shorter than that of carbon because of small emission energy at the wall temperature (typically ~ 0.05 eV) compared with the energy of physical sputtering (average energy 10 eV). A pioneering work on such transport of methane was carried out by Langer [46], followed by Behringer [47]. The rate coefficients for dissociation processes were extensively compiled by Ehrhardt and Langer [48]. Fig. 6 shows the C II line intensity profiles calculated with the IMPMC code compared with measurements in JT-60U [43]. A good agreement with measurement was obtained by including chemical sputtering. It should be noted that there is a large scatter in laboratory data of chemical sputtering yield [38], and that the reaction rates of methane breakup contain uncertainties [48]. There also exits some uncertainty in the parameters of the thin plasma diffusing through the separatrix surface into the private region. In spite of such uncertainties, the conclusion is unchanged: Only chemically sputtered carbons due to neutral particles from the private wall can contribute to the C II line intensities near the X-point.

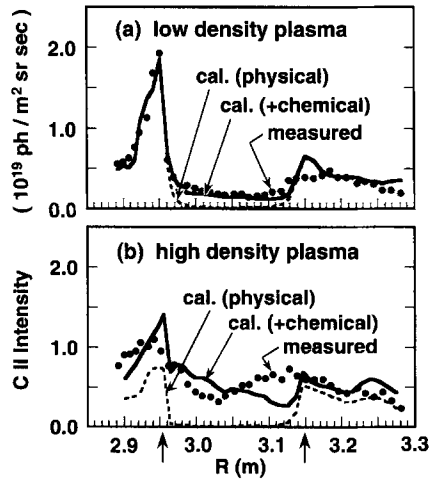

Fig. 6. Calculated profile of C II line intensity in the divertor area for a low density plasma (a) and for a high density plasma (b). The measured profile is plotted with closed circles. The arrows indicate the positions of the separatrix hit points. The experimentally measured intensity near the X-point cannot be explained without chemical sputtering (taken from JT-60U simulations with IMPMC [43]).

Note that the C II intensity of chemical sputtering from the divertor plates is small compared to that from the private wall, although the amount of sputtered methane from the plates (typically, $1-2\times10^{21}$ m^{-2} s^{-1}) is much higher than that from the private wall ($0.2-0.4\times10^{21}$ m^{-2} s^{-1}). This is due to the difference in the generation rate of C^+ ions from methane, which strongly depends on the location of sputtering. Only 10% of methane released from the target plates can become C^+ ions. The methane molecules dissociate at the vicinity of the plates (typically within < 1 mm) and the molecular fragments quickly return to the plates through the diffusion process. Additionally, some of the remaining neutral hydrocarbons return to the plate or wall with some probability (typically ~ 0.5) by randomization of its velocity at neutralization. In contrast, a half of methane released from the wall is dissociated to C^+ ions finally, since they are dissociated away from the target plates. These carbon impurities penetrate into the upstream and the main plasma, and enhance the radiation there. This enhanced radiation near the X-point could trigger a MARFE. To reduce the radiation near the X-point, it is necessary to drop the neutral flux onto the wall. One method is to close the private region with a dome-like structure. Its effect on impurity shielding will be discussed in Section 5.4.

The carbon production in JET was analyzed with the DIVIMP code [49]. The dissociation process of methane was not simulated. Instead of methane, slow carbon atoms were emitted from the target plate with an amount of methane chemically sputtered by D^+ ions. The C II intensity calculated with chemical sputtering was too high compared with the measurement. From this result, however, it cannot be concluded that chemical sputtering is ineffective, because in this calculation the fraction of methane breakup to produce C^+ ions was implicitly assumed to be 1.0. From the comparison with the measurement, the fraction was estimated to be 10%. This low efficiency of producing carbon ions from methane is consistent with that found in the IMPMC simulation. The calculated C II radiation profile disagreed with measurement in the private region and away from the hit points, which may indicate the existence of methane sputtered by neutral particles. Using the DIVIMP code including such impurity source, the carbon production and the net erosion were simulated with the most recent chemical sputtering data. The analysis results showed that the efficiency of producing carbon ions from methane was around 20% at the target and that the gross erosion was reduced significantly due to redeposition [50]. The simulation with the EDGE2D fluid code was also carried out for high density divertor plasmas [51,52]. Instead of physical sputtering, carbon was assumed to be sputtered uniformly from the divertor plates to match the bolometer measurement. A good agreement was obtained in the case of a yield being set as 0.2%. This yield greatly exceeds that of physical sputtering but is smaller than that of chemical sputtering

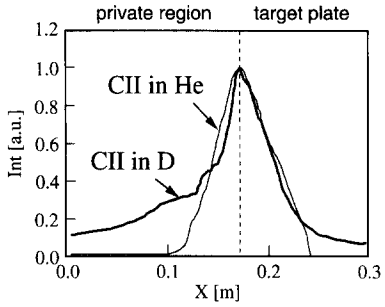

Fig. 7. C II line intensity profile measured radially across the outer target plate. Bold line represents C II intensity in a deuterium discharge, and thin line represents C II intensity in a He discharge (taken from ASDEX-U experiments [54]).

(2–5%) by a factor of 10 or more. Again, it is considered that this factor corresponds to the efficiency of producing carbon ions from methane.

An extensive experimental study for molecular impurities has been carried out in ASDEX-U [53,54]. For standard ohmic discharges, the DIVIMP simulations showed that physical sputtering alone could not explain the C II line intensity observed in the private region [55]. The source with low energy, possibly caused by chemical sputtering turned out to exist. In a completely detached divertor plasma, where the plate temperature was too low for physical sputtering, the C II line intensity was observed to be strong near the X-point [56]. It was concluded that chemical sputtering from the wall due to low energy neutral particles was the major cause of the carbon production in the CDH-mode plasma. A more direct evidence for chemical sputtering was obtained from comparison of He and deuterium discharges [54]. In He discharges where chemical sputtering does not occur, the C II radiation profile in the private region certainly shrinks as shown in Fig. 7. And little difference in the C II profile near the separatrix hit points was observed. This fact confirms again that the efficiency of producing carbon ions from methane is small at the plates. A reasonable agreement between the measured bolometer and simulation with the B2-EIRENE code was obtained for the CDH-mode plasma [57]. Although the dissociation process of methane was modeled similarly to the IMPMC code, the chemical sputtering yield had to be lowered by a factor of > 10 in order to avoid a radiation collapse. Chemical sputtering yields was set to be 0.02 at the wall and < 0.002 at the target plates. Since the plasma temperature is too low (< 5 eV), the methane molecules could dissociate at the place somewhat far from the target plates, increasing the efficiency of producing carbon from methane. Therefore, the methane sputtered from the target plate would contribute to the divertor radiation significantly, unlike the JT-60U result.

3.2. Wall source and impurity puffing

Analysis with the DIVIMP code demonstrated the importance of wall source in ohmic JET discharges [58]. Fig.

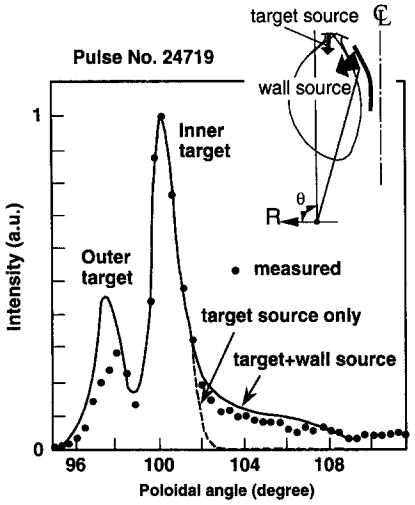

Fig. 8. Comparison of C II line intensity between the measured (closed circle) and calculated profiles for target source only (broken line), and for target source and wall source (solid line). Simulation analysis indicated the existence of wall source (taken from JET simulations with DIVIMP [58]).

8 shows the comparison of C II line radiation between measurement and calculations. The dashed line represents the calculated profile including only the target source, i.e., physical sputtering and self-sputtering. The profile near the target agrees well with the measurement. However, the tail observed away from the inner target cannot be explained by the target source only. Assuming a wall source, the tails seen on both C II and C IV line intensity profiles were reproduced. The wall source was assumed to exist along the inner wall extending as far as the midplane (bold line in Fig. 8). The bombardment of charge exchange neutrals is considered to be the cause of the wall source. Although the total wall source amounted to only 25% of the target source, it contributes about 40–45% of the core impurity content because of penetration probability larger than the target source by a factor of ~ 3. In Alcator C-mod, the contribution of the wall source to the central impurity content is larger than that of the divertor source by a factor of 3 [59]. This is caused by the penetration probability for the wall source which is roughly 10 times larger than that for the divertor source. Hence the wall source must be reduced in order to improve the core plasma purity.

In early DIII-D VH-mode experiments, it was reported that impurity accumulation during the VH-mode was not observed in contrast to the ELM-free H-mode. This was attributed to screening by a thick SOL [60]. However, more recent data from improved impurity diagnostics showed a continual influx of carbon, the dominant impurity, that was at least as large as during ELM-free H-mode [61]. (Furthermore, a thick SOL was not usually present during VH-mode [62].) Since the intrinsic impurities are generated from the target as well as from the wall, it is difficult to distinguish the screening effect of the SOL against the wall source.

In Alcator C-mod, the screening process was studied using impurity injection of argon and nitrogen [63,64], with which the impurity source was controlled independently of the production process. For a non-recycling impurity (e.g., methane, nitrogen), the core impurity content is determined by the balance between the influx and the loss rates associated with the flow to the target. In fact, the total number of impurities in the main plasma was found to be proportional to the impurity injection rate. It was also found that the fueling efficiency, defined as the impurity number in the main plasma normalized to the influx, decreased with increasing plasma density until the plasma detached from the target. The screening was significantly reduced in the detached plasma. It was confirmed that the screening due to a high density and high temperature SOL is important to reduce the impurity content in the main plasma. The screening in the SOL of the limiter discharges was also discussed in a review paper by Montier-Garbet [65].

4. Impurity shielding and cross field diffusion

The impurity contamination in the main plasma is determined by production, transport in the SOL, and transport in the main plasma. In this section, the second issue (i.e., the parallel motion of impurity ions and the cross field diffusion in the SOL) is addressed. The parallel force acting on an impurity ion consists of the electric force, the friction force and the thermal force with the background plasma:

$$m_{\mathrm{I}}\frac{\mathrm{d}v_{Z\|}}{\mathrm{d}t} = F_Z = Ze E_{\|} + m_{\mathrm{I}}\nu_Z\left(V_{\|} - v_{Z\|}\right) + \alpha_Z\frac{\partial T_{\mathrm{e}}}{\partial s} + \beta_Z\frac{\partial T_{\mathrm{i}}}{\partial s}, \tag{3}$$

where Z is the charge number, $E_{\|}$ is the electric field parallel to the field line, $V_{\|}$ is the plasma flow velocity parallel to the field line and ν_Z is the impurity-ion collision frequency. The coefficients of thermal force, α_Z and β_Z, described in Ref. [17], are close to $0.71Z^2$ and $2Z^2$, respectively, under the approximation of $m_{\mathrm{I}} \gg m_{\mathrm{i}}$. In fluid codes, the impurity pressure gradient force, $-n_Z^{-1}\partial p_Z/\partial s$ (n_Z and p_Z are impurity density and pressure, respectively) is added to RHS of Eq. (3). In Monte Carlo codes, the pressure gradient force is not included explicitly in the equation of motion, because it results from random velocities of individual particles.

Normally, the friction force and the electric force push impurity ions to the target plate. In high recycling divertor plasma, however, flow reversal appears in some region and may entrain impurity ions towards the upstream. The

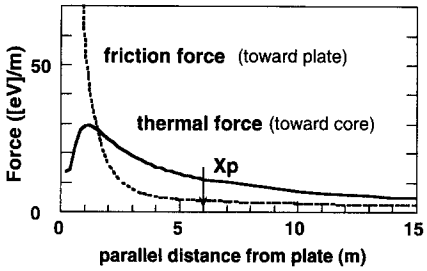

Fig. 9. Parallel forces acting on impurity ions along a magnetic field line. They are calculated using plasma parameters shown in Fig. 3. Note that such force balance strongly depends on the divertor characteristics.

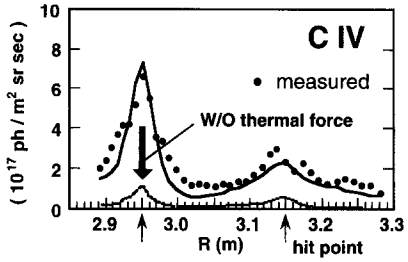

Fig. 10. Comparison between measured C IV intensity profile in the divertor area (closed circles) and the calculated profiles with thermal force turned on (solid line) and with thermal force turned off (broken line). The presence of thermal force was clearly demonstrated (taken from simulations of a JT-60U low density plasma with IMPMC [29,70]).

collision frequency with the background plasma in the downstream (colder region) is higher than that in the upstream (hotter region) because of the temperature dependence of Coulomb collision ($\nu \propto T^{-3/2}$). As a result, the force by plasma ions coming from the downstream is stronger than that from the upstream. The resultant force (i.e., the thermal force) pushes the impurity ions to the upstream. Impurity retention in divertor is determined by the balance of these forces on impurities. The ion temperature gradient is higher than that of electron (see Fig. 3) due to the mass dependence of the parallel conductivity ($\chi_{\|} \propto m^{-1/2}$), provided that the heat fluxes across the separatrix are not so different between ion and electron channels. Thus the ion thermal force is larger than the electron thermal force and the electric force. Although strongly depending on the divertor characteristics, the force balance is demonstrated in Fig. 9 to draw a rough picture about impurity retention. The plasma parameters are those shown in Fig. 3. Note that the net force pushes the impurity ions toward the core plasma everywhere except the vicinity of the target plate. What is worse, in the high recycling divertor plasma, the gradient of T_i increases and flow velocity in the upstream decreases. Therefore, the enhanced friction force which overcomes the thermal force is required to suppress the core impurity contamination. The methods to increase the plasma flow will be discussed in the next section.

Impurity retention is very much complicated because the forces on impurities strongly depend on the plasma parameters, which significantly vary in the SOL, (especially gradient of temperature). A simple prescription for impurity retention, even if it is a rough estimation, would be very useful in predicting the plasma condition required to retain impurities, although it is not easy to accomplish this task. The first attempt has been made by Stangeby and Elder [66,67]. From a 1D fluid theory with simplified assumptions, a simple analytic description was derived. The leakage flux out of the divertor was found to vary as $\exp(-C/T_d^2)$ where T_d is the plasma ion temperature at the target. The threshold temperature T_d^{thr} at which the leakage flux becomes significant was found to vary as $T_d^{thr} \propto (n_e \lambda_i)^{1/2}$ where λ_i is the characteristic scale length of hydrogen ionization. These predictions were examined by using the DIVIMP code. A close agreement was found for plasma conditions that are strongly collisional, but for weaker collisionality the prediction is found to overestimate leakage.

For the predicted forces acting on impurities similarly to Fig. 9, neon impurity transport in the DIII-D tokamak was simulated [68] with a 1D fluid model, NEWT1D [69]. When the impurity was injected where the thermal force dominated, neon was found to build up above the X-point. Both the Stangeby criteria and this result clearly indicate that the impurity shielding strongly depends on the ionization location of impurity neutrals.

The effect of parallel forces on shielding was investigated experimentally for a low density plasma of JT-60U [29,70]. The impurity production was successfully reproduced by deuterium physical sputtering and self-sputtering (see Fig. 6(a)), which enabled investigation of impurity transport. As shown in Fig. 10, the comparison between the measured C IV intensity profile and the profile calculated with the IMPMC code was made. When the thermal force was turned off in the simulations, the calculated intensity was significantly reduced. Thus the presence of thermal force was confirmed experimentally. The effect of the forces on the penetration probability is listed in Table 2. When all forces are active, 17% of test particles is found

Table 2
Effect of parallel forces on impurity shielding. Probability of penetration into the main plasma is strongly enhanced by the thermal force (taken from simulations of a JT-60U low density plasma with IMPMC [29])

Case	Probability
All force	17%
W/O thermal force	< 1%
W/O electric force	23%
W/O friction force	47%
All force assuming $T_i = T_e$	< 1%

to enter the main plasma, which is much higher compared with the 1D simple case (~ 2%) shown in Fig. 3. Since impurity neutrals are ionized far from the target plate in this case, many ions are pushed towards the upstream by the thermal force. In fact, when the thermal force is turned off, the probability is reduced to less than 1%. Also in the calculation with the assumption of $T_i = T_e$ in the SOL, the probability becomes also less than 1%. This result indicates that the impurity shielding is sensitive to the ion temperature profile near the divertor plate.

The impurity ions carried above the X-point by the thermal force can enter the main plasma through the cross field diffusion process. The diffusion coefficient of impurity ions was evaluated. The ionization time of C^+, which is typically $\leq 10^{-5}$ s near the plate, is shorter than the diffusion time ($\tau_{diff} > 10^{-5}$ s for mean displacement of 1 cm for the expected value of $D_\perp < 5$ m^2/s). Indeed, Fig. 11(a) shows that the C II line radiation profile is insensitive to the diffusion process. On the other hand, the ionization time of C^{2+} and C^{3+} is comparable to the diffusion time, therefore the C IV line radiation profile reflects the diffusion process, as shown in Fig. 11(b). The comparison with the measurement indicated that the diffusion coefficient was around 1 m^2/s. The probability of penetration into the main plasma was found to change a little from 18% to 14% by variation of $D_\perp = 0.5$–5 m^2/s in the SOL. However, it should be noted that the impurity core content is governed by influx from the SOL and transport ($D_\perp$ and V_{pinch}) in the main plasma. The impurity transport in the main plasma is very important for the core contamination, but is out of the scope of this paper. This issue was addressed in review papers [16,37,71,72].

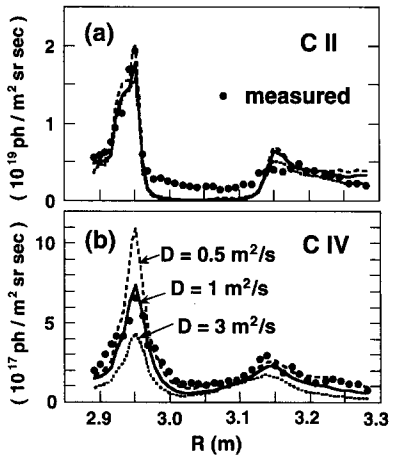

Fig. 11. (a) C II line intensity profiles in the divertor area. The calculated profiles were insensitive to the diffusion coefficient $D_\perp$ in the range of 0.5–3 m^2/s. (b) C IV line intensity profiles calculated with various values of $D_\perp$. The comparison with the measurement (closed circles) indicated that the diffusion coefficient was around 1 m^2/s (taken from simulations of a JT-60U low density plasma with IMPMC [29]).

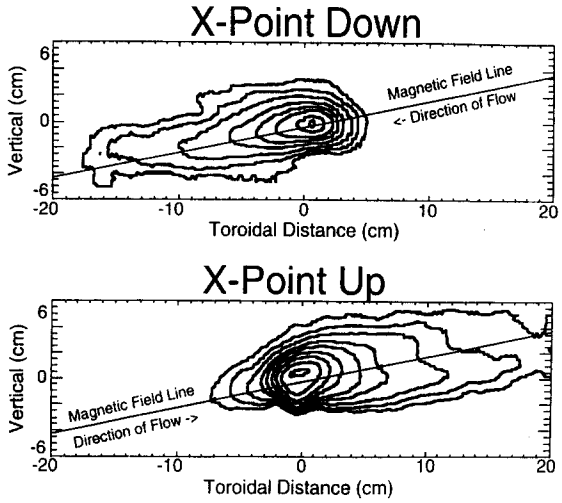

Fig. 12. Spatial distribution of C II intensity during methane gas puffing at inner-wall midplane observed with a CCD camera located outside midplane vessel. The density of C^+ ions was clearly shifted along a magnetic field line toward the target plates in upper and lower X-point discharges (taken from Alcator C-mod experiments [74]).

The parallel flow of carbon impurities towards the divertor plate at the midplane was directly observed in the Alcator C-mod tokamak [73,74]. Fig. 12 shows the spatial distribution of the C II intensity during methane gas puffing from the inner wall midplane observed with a CCD camera. The density of C^+ ions is clearly shifted toward the divertor plate. From this displacement, the flow speed of impurities was found to be typically 1.2×10^4 m/s, corresponding to Mach number of 0.3 with electron temperature of 20 eV. The existence of such a high flow speed at the upstream in high density discharges ($\bar{n}_e = 1.5$–2×10^{20} m^{-3}) without pumping is a very encouraging result for impurity retention in future tokamaks. The density in the SOL ($n_S \sim 2 \times 10^{19}$ m^{-3}) was relatively low compared to the main plasma density. If the low density in the SOL or the device size is essential, it might be difficult to obtain high flow speed in ITER with $n_S \sim 8 \times 10^{19}$ m^{-3}. The measurement of flow velocity in large tokamaks, such as JET and JT-60U, is strongly desired.

5. Impurity control

Several methods for impurity control to retain impurities in the divertor region, to enhance the divertor radiation, and to reduce the impurity content in the main plasma, have been proposed. Applying some methods to experiments, good results have been obtained, for example, by means of divertor biasing and ergodic divertor. Such experimental results are not discussed in this paper, which are described in review papers [65,75], respectively.

In this section, we discuss the optimum impurity species for enhancing divertor radiation, impurity control by gas puffing and divertor pumping, and optimization of divertor geometry for impurity shielding.

5.1. Species of impurity puffing

It has been widely recognized that impurity injection is needed to obtain the radiative divertor. Integrating the heat conduction equation including impurity radiation along the field line in the SOL, the impurity condition required to obtain the detached plasma was derived analytically [76]. The criteria of the impurity fraction were investigated for Be, C, Ne and Ar. The impurity radiation is significantly enhanced by the recycling and charge exchange recombination compared with that for a coronal equilibrium. Thereby it may be possible to achieve the heat exhaust required in ITER. The simple analysis also showed that argon has the highest loss rate, but the allowed fraction is the smallest among the four impurities. For the choice of impurity species, there are two important factors to be taken into consideration: enhancement of edge radiation, and avoidance of core radiation and fuel dilution. The most effective radiator was found to be neon in this simple analysis. On the contrary to the expectation, the lowest dilution in the core plasma was achieved in the discharge with argon puffing in JET [7]. The radiation profile depends not only on electron temperature but also on the transport in the main plasma and the SOL, and the recycling condition at the target plate and wall. Such effects lead to the difference between the simple analysis and the experimental result. An index for estimating the effectiveness as a radiator provides us useful information about choice of impurity puffing. One of such indexes for estimating the optimum radiation profile both at the divertor plasma and the main plasma may be the parameter of $P_{\mathrm{rad}}^{\mathrm{div+SOL}}/P_{\mathrm{rad}}^{\mathrm{main}}$, where $P_{\mathrm{rad}}^{\mathrm{main}}$ and $P_{\mathrm{rad}}^{\mathrm{div+SOL}}$ are radiation inside and outside the separatrix, respectively. In terms of this parameter, the highly radiating discharges with Ne, Ar and N_2 injections were compared for ASDEX-U [77]. The most favorable (i.e., high) value was obtained in the discharge with N_2 puffing. Also, the radiation profile strongly changes depending on attached or detached condition. JET, for example, reported that the ratio of divertor radiation to bulk radiation, $P_{\mathrm{rad}}^{\mathrm{div}}/P_{\mathrm{rad}}^{\mathrm{main}}$, decreases from ~ 1.3 in an attached plasma to ~ 1.4 in a detached plasma [3].

To investigate the possibility of applying the impurity injection scenario to ITER, the scaling study for the relationship between Z_{eff} and P_{rad} has just been started by Matthews et al. [78]. According to this scaling based on the experimental results from Alcator C-mod, ASDEX, ASDEX-U, DIII-D, JT-60U, the prediction of Z_{eff} for ITER was 1.6, which is not far away from the ITER requirement of $Z_{\mathrm{eff}} < 1.2$ excluding the contribution from He ash. In fact, the ITER requirement was within the scatter of the existing data. The scaling showed a weak dependence on Z ($Z_{\mathrm{eff}} - 1 \propto Z^{0.19} P_{\mathrm{rad}}$). In the scaling study for this Z dependence, more careful choice of data points may be needed and collection of new data for various injection species is strongly called for. Since the fuel dilution is the most severe condition for ITER rather than the radiation in the main plasma, the dependence of additional radiated power per Z_{eff} increment ($\Delta P_{\mathrm{rad}}^{\mathrm{div+SOL+edge}}/\Delta Z_{\mathrm{eff}}$, where $\Delta P_{\mathrm{rad}}^{\mathrm{div+SOL+edge}}$ is the increase in radiation power excluding the core by impurity injection) is more important for choice of impurity species.

5.2. Enhancement of plasma flow by puff and pump

One means of impurity retention is to enhance the plasma flow by injecting D_2 gas into the upstream SOL and pumping the D_2 gas from the divertor region simultaneously. The effect of plasma flow on core impurity content was first demonstrated in Doublet-III discharges with puff and no active pump (but effective wall pumping) [79], followed by the puff and pump experiment in DIII-D [80,81]. Similar experiments were performed on JET [82] and ASDEX-U [83,84] and recently, again on DIII-D [85]. JET reported that the plasma flow induced by fueling and pumping showed little influence on the core concentration of neon impurity, independently of the impurity puff location: at the top of the plasma or into the divertor [82]. A plausible explanation was that neutral leakage from the divertor region showed a stronger effect on the SOL plasma flow than fueling ($\sim 5\%$ target flux), indicating that neutral leakage must be suppressed with a closed divertor to distinguish the effect of puff and pump. In both DIII-D and ASDEX-U experiments, the core impurity contents were reduced by puff and pump, but the explana-

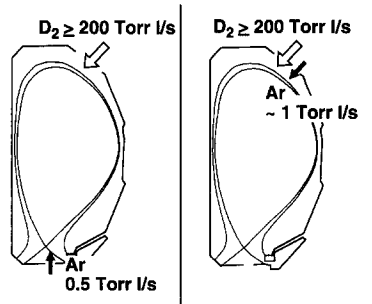

	W/O	W D_2 Puff	W/O	W D_2 Puff
n_{Ar}(core) ($10^{16}m^{-3}$)	5.6	0.29	19	2
τ_{Ar} (ms)	20	1	40	4

Fig. 13. Schematic diagram and analysis results of the puff and pump experiment in DIII-D. Central Ar density n_{Ar}(core) and effective confinement time of Ar, defined as τ_{Ar} = (number of Ar ions in plasma)/(Ar atom puff rate), are evaluated with MIST code (taken from DIII-D experiments [81]).

tions of improved impurity retention were different. This crucial issue is also discussed in a review paper by Bosch et al. [86].

Fig. 13 shows the schematic diagram of the puff and pump experiment in DIII-D [81]. Argon was puffed either into the private region or near the top of the plasma. The argon transport was investigated by comparing the discharges with and without strong deuterium puffing and pumping. The argon densities were evaluated from comparison of the measured and calculated Ar line intensity with the 1D impurity fluid code (MIST) [87]. In discharges with puffing and pumping, the central argon densities were found to be significantly reduced by a factor of 20 or 10, depending on the location of gas puffing. The reduction in the core impurity content by D_2 puffing was considered to be attributed to the enhancement of the plasma flow in the SOL. It should be noted that the core plasma parameters and the ELM activity were changed by strong puffing. Since such changes affect impurity transport in the periphery of the main plasma, it is difficult to determine which effect played an essential role on the reduction of impurity content.

In ASDEX-U, the exhaust rate for Ne and Ar was found to depend strongly on the neutral gas density in the divertor [83,86,88]. However, the good impurity exhaust was considered not to be attributed to the upstream plasma flow induced by external gas puffing, rather to the high divertor neutral gas density. To separate the effects of the divertor neutral density and the plasma flow, another experiments with the neutral gas density kept constant by feedback-controlled puffing were performed [84]. In these discharges with almost the same plasma profiles in the SOL, the identical impurity retention was obtained, despite the different pumping speed by a factor of ~ 4. These experimental results concluded that the impurity retention depended mainly on the divertor neutral gas density, little on the external D_2 puffing, in contrast to DIII-D conclusion. Recently TdeV also obtained a similar result, showing impurity compression improved with increasing divertor neutral pressure [89]. A simulation analysis with B2-EIRENE code was carried out for exhaust experiments in ASDEX-U and successfully reproduced the dependence of compression factor for He and Ne on neutral flux density [86,90]. It was found that the plasma flow in the divertor region was enhanced by internal recycling near the target and the recirculation in the divertor chamber with increasing the divertor neutral gas density, and that this enhanced plasma flow increased the impurity retention in the divertor.

What caused the difference between the DIII-D results and the ASDEX-U results? The ASDEX-U results indicate that the upstream flow externally induced has little effect but the flow in the divertor region plays a significant role on the impurity retention. The upstream plasma flow becomes less important in a high density and high temperature SOL because of the high shielding effect. In fact, the SOL parameters of ASDEX-U are $n_e = 5 \times 10^{19}$ m^{-3}, $T_e = 100$ eV [84], while those of DIII-D are $n_e = 1.5$–2×10^{19} m^{-3}, $T_e = 40$ eV [85]. Besides, the following difference can cause the different results: the geometry effect, or the plasma confinement mode (H-mode with Type I ELMs versus CDH-mode with Type III ELMs), or the location of the impurity gas puffing (private region versus outer midplane of the main chamber). As for the confinement mode, recent ASDEX-U results observed no clear difference in decay rates of He for H-mode and CDH mode discharges [91]. In addition, Alcator C-mod reported that the core density of recycling impurities (such as Ar and Ne) was independent of the poloidal position of injection [64]. Therefore, an alternative explanation is that the effect of the externally induced plasma flow might be masked by a large neutral leakage from the ASDEX-U divertor because of open divertor configuration, as pointed out in the JET experiments [82]. To conclude the effect of puff and pump on the plasma flow, more experiments with direct measurements of the plasma flow in the upstream region and the divertor region are needed.

Recently, divertor exhaust enrichments were measured more directly in DIII-D [85]. The exhaust enrichment factor was defined by

$$\eta_{exh} = \left(p_{Ne}/2p_{D_2} \right)^{div} / \left(n_{Ne^{+10}}/n_e \right)^{main}, \quad (4)$$

where Ne^{+10} was measured by absolutely calibrated charge exchange recombination spectroscopy. The experimental results showed that D_2 puff into the SOL with pump increased the Ne exhaust enrichment factor by 2–3 times compared to the discharge without pump or the discharge with D_2 puff into the private region with pump. It was confirmed again that the upstream plasma flow is important for impurity enrichment in the DIII-D divertor.

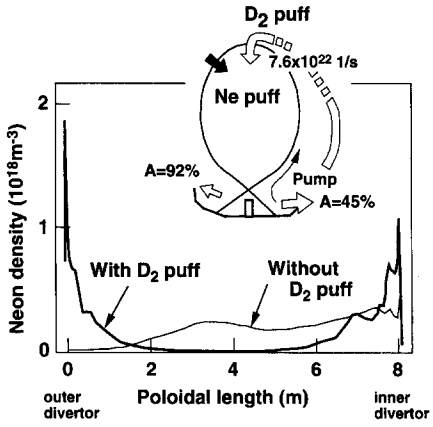

Fig. 14. Poloidal variation of neon density calculated with EDGE2D for planned JET divertor (MARK IIGB). Neon impurities injected uniformly from the walls. They were retained in the divertor with the plasma flow induced by deuterium puffing and pumping near the targets, as shown by thick solid line. The albedoes at the inner and outer divertor box were 92% and 45%, respectively (taken from JET puff and pump simulations [92]).

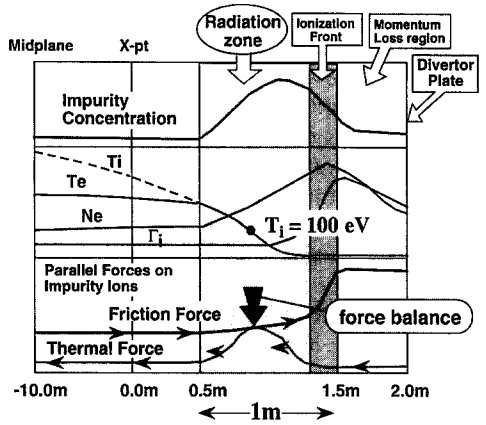

Fig. 15. Radiative divertor concept for ITER. To retain impurities in the divertor (as shown in the top figure), the friction force must be balanced at least with the maximum of thermal force in the radiation zone (as shown in the bottom figure). The middle figure shows the plasma parameters. From this force balance, the required fuel gas flow rate was evaluated (taken from in Ref. [93]).

The puff and pump experiments on the planned JET divertor (MARK IIGB) were simulated using the EDGE2D code [92]. Neon was injected uniformly from the walls. Fig. 14 shows the poloidal variation of neon density. Without an induced plasma flow, injected neon was accumulated near the SOL midplane. When the plasma flows were induced by deuterium puffing into the upstream SOL and pumping near the targets, the neon impurities were remarkably retained in the divertor.

5.3. Fuel gas flow required in ITER

Although not all the experiments have confirmed that the plasma flow upstream induced by puff and pump can improve the impurity retention, simulations have clearly demonstrated its effects. Stambaugh evaluated the fuel gas flow required to retain impurities in ITER from simple consideration [93]. Fig. 15 illustrates the radiative divertor concept. Most of the power from the upstream is removed by the impurity radiation, in a region from 0.5 m to 1.5 m below the X-point. The electron and ion temperatures decrease to less than 10 eV at the end of the radiation zone, and an ionization front is located there. Below this front, the plasma momentum is removed by charge exchange with neutrals. The remaining power or momentum impinging on the target plates is too small to cause serious damage or erosion.

To retain impurities in the divertor, the friction force must overcome the thermal force everywhere. The friction force must be balanced at least with the maximum of thermal force in the radiation zone. The parallel flow $\Gamma_{i\parallel} = n_i V_\parallel$ was roughly evaluated from the force balance equation, $m_I \nu_Z V_\parallel = 2Z^2 \nabla_\parallel T_i$. To obtain the total flow, $\Gamma_{i\parallel}$ was integrated across the SOL assuming exponential falloffs of the density and temperature profiles. The required fuel gas flow rate evaluated ($\dot{N} \propto T_i^{5/2}/l_{T_i}$ where l_{T_i} is the ion temperature gradient scale length) was 800 Pa m^3/s for reasonable operating point of $T_i = 100$ eV and $l_{T_i} \approx 1$ m. Excessive gas flow causes new serious problems, that is, tritium inventory and sputtering by charge exchange neutrals. Since an acceptable value is about 200 Pa m^3/s, the value of 800 Pa m^3/s appears to be impracticable. However, the analysis with 1D model shows that neutral recirculation inside divertor region could reduce the required fuel flow rate to 40 Pa m^3/s [94]. Further simulation analysis with 2D divertor code is needed to investigate the feasibility.

5.4. Effect of divertor geometry

Experiments with strong gas puffing of deuterium and light impurity have been widely performed to obtain a strong radiative divertor. However, the energy confinement and/or the core plasma purity have been degraded by the back flow of neutral particles and/or impurities into the main plasma. In order to achieve high performance of the main plasma with strong radiative divertor, such a back flow must be suppressed by closing the divertor with baffles and domes. Therefore, a divertor modification to a closed divertor has been accomplished on Alcator C-mod and is being planned on ASDEX-U, DIII-D, JET and JT-60U.

For a variety of baffle geometry in the planned ASDEX-U divertor, the effect of baffle on the plasma flow

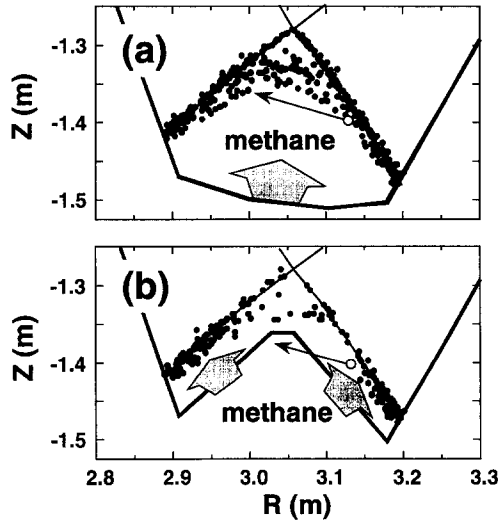

Fig. 16. Birth positions of C^+ ions dissociated from methane, (a) in the open divertor (without a dome), and (b) in the W-shaped divertor (with a dome). Methane is released from the private region by charge exchange neutrals. Note that the dome drastically suppressed the production of carbon impurities around the X-point (taken from simulations for new JT-60U divertor [99]).

was recently investigated with the B2-EIRENE code [95,96]. The private flux baffle suppressed the flow reversal, but its influence was found to be very small on the impurity retention. This result may be consistent with the previous analysis of DIVIMP, showing the flow reversal did not enhance the back flow of impurities sputtered at the target [97].

JT-60U has a plan to modify the present open divertor to a new semi-closed divertor with a dome [70,98]. In an open divertor, chemically sputtered carbons from the private region were found to enhance the radiation around the X-point, and possibly lead to an X-point MARFE [43]. The shielding effect of a dome was investigated with the IMPMC code [99]. Methane is sputtered due to chemical sputtering by charge exchange neutrals. The neutral flux onto the wall was calculated by a 2D neutral transport code to evaluate the methane outflux. In the divertor without a dome, methane outflux spread over the private region, while in the divertor with a dome, they were confined to the lower region near the target plates. Then dissociation processes were simulated with the IMPMC code. Fig. 16 shows the birth positions of C^+ ions from methane for the divertor with and without the dome. Generation probability of C^+ ions from methane was reduced from 43% to 25% by the dome. It should be noted that the dome drastically suppressed the carbon impurity flux around the X-point. As a result, the radiation near the X-point was reduced by a factor of ~ 2. Furthermore, the temperature dependence of the radiation was found to have the opposite sign. The radiation for the case without the dome increased with decrease of T_e. On the other hand, in the divertor with the dome which suppressed impurity influx into the upstream SOL, the radiation decreased with T_e reduction, suggesting that the dome is effective in stabilization of a MARFE caused by chemically sputtered carbon impurities. This interesting result should be confirmed with a self-consistent modelling of the divertor plasma and impurity transport.

6. Summary

Recent advances in diagnostics and simulation codes have allowed significant progress in understanding of the impurity production and transport in SOL and divertor.

– The assumptions used in fluid models, i.e., instantaneous thermalization of impurity ions and simplified evaluation of self-sputtering outflux, are examined with a 1D Monte Carlo code. In high density plasmas, impurity ions with low charge states become dominant in ions returning to the target plates. Since the assumptions can not be applied for such ions, impurity flux into the main plasma is overestimated in fluid models.

– The production mechanism of carbon, which is the dominant impurity in most of the present tokamaks with carbon divertor plates and/or walls, has been investigated extensively. It was found that in the low recycling divertor, physical sputtering and self sputtering are the main causes of carbon generation. It is confirmed that chemical sputtering from the wall and/or the target plates becomes dominant in carbon production mechanism in high recycling and detached divertor plasmas.

– The efficiency of dissociation to carbon ions from methane strongly depends on the location of sputtering, that is, only 10% at the target plates and 50% for methane sputtered by charge exchange neutrals hitting the private wall. The small efficiency at the target results from prompt redeposition of molecular fragments, which implies that the chemical erosion of target plates is effectively small.

– The wall source is found to contribute to the core impurity content because of a large penetration probability. Influx of the wall source into the main plasma can be suppressed by a high density and high temperature SOL plasma.

– Impurity retention in the divertor is determined basically by the balance between the thermal force and the friction force. From the measured C IV radiation profile, the impurity diffusion coefficient was evaluated as ~ 1 m^2/s in JT-60U L-mode low density plasma.

– One of the most promising methods for impurity control is to enhance the plasma flow with gas puffing and pumping. In puff and pump experiments in DIII-D and ASDEX-U, impurity retention in the divertor was improved. However, which effect is more effective for impurity retention, the upstream plasma flow induced externally or recirculation of neutrals in the divertor chamber, is still an open question. Direct measurement of the plasma flow is needed to resolved this crucial issue.

– Methane sputtered from the private region is found to enhance the radiation around the X-point in an open divertor, and has a possibility to cause an X-point MARFE. A dome to close the private region effectively suppresses the carbon impurity flux into the upstream SOL and the temperature dependence of its radiation power becomes favorable to thermal stability ($\delta P_{rad} < 0$ for $\delta T_e < 0$), suggesting that the dome is effective in stabilization of a MARFE caused by chemical sputtering.

Acknowledgements

The authors are grateful to Dr M. Shimada for his continuous encouragement and helpful discussions. Useful suggestions from Dr N. Hosogane, Dr N. Asakura, Dr K. Itami, Dr R. Yoshino and Dr M. Azumi are gratefully acknowledged. They would like to thank Professor P.C. Stangeby and Dr G.F. Matthews, Dr H.Y. Guo, Dr A. Loarte, Dr J. Neuhauser, Dr H.-S. Bosch, Dr A. Kallenbach, Dr D. Naujoks, Dr M.J. Schaffer, Dr M.E. Fenstermacher, Dr T.E. Evans, Dr R.D. Stambaugh, Dr G.M. McCracken, Dr B. Lipschultz, Dr C.S. Pitcher, Dr A. Grosman, Dr P. Monier-Garbet, Dr J.W. Davis, Dr M. Sugihara, Dr S. Tsuji-Iio and Dr S. Ohtsu for fruitful discussions and useful comments.

References

[1] G. Janeschitz, Plasma Phys. Control. Fusion 37 (1995) A19.
[2] S.L. Allen et al., J. Nucl. Mater. 220–222 (1995) 336.
[3] G.F. Matthews and the JET team, Plasma Phys. Control. Fusion 37 (1995) A227.
[4] B. Lipschultz, J.A. Goetz, B. LaBombard, G.M. McCracken, H. Ohkawa, Y. Takase and J.L. Terry, these Proceedings, p. 771.
[5] O. Gruber et al., Phys. Rev. Lett. 74 (1995) 4217.
[6] K. Itami et al., in: Proc. 16th Int. Conf. Plasma Phys. Contr. Nucl. Fusion Res., Montréal, Canada, IAEA-CN-64/A-4-2 (1996).
[7] M. Keilhacker and the JET team, Plasma Phys. Control. Fusion 37 (1995) A3.
[8] B.L. Stansfield, J. Nucl. Mater. 220–222 (1995) 1121.
[9] B. LaBombard et al., these Proceedings, p. 149.
[10] S.L. Allen et al., these Proceedings, p. 595.
[11] R. Reichle et al., in: Proc. 22nd EPS Conf. on Controlled Fusion and Plasma Physics, Vol. 19C, Part III (1995) p. 85.
[12] J.C. Fuchs et al., in Proc. 22nd EPS Conf. on Controlled Fusion and Plasma Physics, Vol. 19C, Part III (1995) p. 401.
[13] C. Kurz et al., J. Nucl. Mater. 220–222 (1995) 963.
[14] S.L. Allen et al., Plasma Phys. Control. Fusion (1995) A191.
[15] M.E. Fenstermacher et al., these Proceedings, p. 666.
[16] P.C. Stangeby, Contrib. Plasma Phys. 28 (1988) 507.
[17] J. Neuhauser et al., Nucl. Fusion 24 (1984) 39.
[18] J. Neuhauser et al., J. Nucl. Mater. 121 (1984) 194.
[19] B. Braams, NET Report Mo. 68, Jan. 1987 (EUR-FU/IXII-80-87-68).
[20] R. Simonini et al., in Proc. 12th EPS Conf. on Controlled Fusion and Plasma Physics, Vol. 9F, Part II (1985) p. 484.
[21] T.D. Rognlien et al., J. Nucl. Mater. 196–198 (1992) 347.
[22] Y. Igitkhanov and V. Pozharov, in: Summary of ITER Specialist's Working Session on Model Validation and Development of Edge Plasma Models. ITER-Th-Ph-9-4 (1989).
[23] N. Ueda et al., Nucl. Fusion 28 (1988) 1183.
[24] A. Loarte, these Proceedings, p. 118.
[25] S. Sengoku et al., Nucl. Fusion 19 (1979) 1327.
[26] J.N. Brooks, Nucl. Technol. Fusion 4 (1983) 33.
[27] J.N. Brooks, J. Nucl. Mater. 145–147 (1987) 837.
[28] P.C. Stangeby and J.D. Elder, J. Nucl. Mater. 196–198 (1992) 258.
[29] K. Shimizu et al., J. Nucl. Mater. 220–222 (1995) 410.
[30] T.E. Evans et al., Proc. of the 10th Int. Conf. on Stellarators, IEA, 22–26 May 1995, Madrid, Spain; T.E. Evans et al., General Atomics. GA-A22064 (1995).
[31] K. Shimizu et al., J. Nucl. Mater. 196–198 (1992) 476.
[32] R.D. Monk et al., J. Nucl. Mater. 220–222 (1995) 612.
[33] P.C. Stangeby, J.D. Elder, W. Fundamenski, A. Loarte, L.D. Horton, R. Simonini, A. Taroni, O.F. Matthews and R.D. Monk, these Proceedings, p. 358.
[34] M.W. Thompson, Phys. Rep. 69 (1981) 335.
[35] J. Roth et al., Suppl. J. Nucl. Fusion 1 (1991) 63.
[36] J. Winter, J. Nucl. Mater. 176&177 (1990) 14.
[37] C. S. Pitcher and P.C. Stangeby, Plasma Phys. Control. Fusion, to be published.
[38] J.W. Davis and A.A. Haasz, these Proceedings, p. 37.
[39] W.O. Hofer and J. Roth, Physical Processes of the Interaction of Fusion Plasmas with Solids (Academic Press, Amsterdam, 1996).
[40] H. Kubo et al., J. Nucl. Mater. 196–198 (1992) 71.
[41] A. Sakasai et al., in: Plasma Physics and Controlled Nuclear Fusion Research 1992 (Proc. 14th Int. Conf. Wurzburg, 1992), Vol. 1 (IAEA, Vienna, 1993) p. 195.
[42] N. Hosogane et al., J. Nucl. Mater. 196–198 (1992) 750.
[43] K. Shimizu et al., in: Plasma Physics and Controlled Nuclear Fusion Research 1994 (Proc. 15th Int. Conf. Seville, 1994), Vol. 3 (IAEA, Vienna, 1996) p. 431.
[44] C. Garcia-Rosales and J. Roth, in: Proc. of 21st EPS Conf. on Controlled Fusion and Plasma Physics, Vol. 18B, Part II (1994) p. 770.
[45] K. Shimizu and T. Takizuka, J. Plasma Fusion Res. 71 (1995) 801.
[46] W. Langer, Nucl. Fusion 22 (1982) 751.
[47] K. Behringer, J. Nucl. Mater. 176&177 (1990) 606.
[48] A.B. Ehrhardt and W.D. Langer, Princeton Plasma Physics Laboratory Report, PPPL-2477 (1987).
[49] H.Y. Guo et al., in: Proc. 22nd EPS Conf. on Controlled Fusion and Plasma Physics, Vol. 19C, Part II (1995) p. 273.
[50] H.Y. Guo et al., these Proceedings, p. 385.
[51] A. Taroni et al., in: Proc. 22nd EPS Conf. on Controlled Fusion and Plasma Physics, Vol. 19C, Part IV (1995) p. 297.
[52] L.D. Horton and the JET team, in: Plasma Physics and Controlled Nuclear Fusion Research 1994 (Proc. 15th Int. Conf. Seville, 1994), Vol. 1 (IAEA, Vienna, 1996) p. 541.
[53] A. Kallenbach et al., Nucl. Fusion 34 (1994) 1557.
[54] W. Poschenrieder et al., J. Nucl. Mater. 220–222 (1995) 36.
[55] K. Krieger et al., J. Nucl. Mater. 220–222 (1995) 548.
[56] A.R. Field et al., in: Proc. 22nd EPS Conf. on Controlled Fusion and Plasma Physics, Vol. 19C, Part II (1995) p. 293.
[57] R. Schneider et al., in: Proc. of 22nd EPS Conf. on Controlled Fusion and Plasma Physics, Vol. 19C, Part IV (1995) p. 285.
[58] G.F. Matthews et al., J. Nucl. Mater. 196–198 (1992) 374.
[59] C. Kurz et al., J. Nucl. Mater. 220–222 (1995) 963.
[60] S.I. Lippmann et al., J. Nucl. Mater. 196–198 (1992) 498.
[61] M.R. Wade et al., in: Proc. 23rd EPS Conf. on Controlled Fusion and Plasma Physics, Vol. 20C (1996).
[62] M.J. Schaffer, private communication (1996).
[63] G.M. McCracken et al., J. Nucl. Mater. 220–222 (1995) 264.
[64] G.M. McCracken et al., these Proceedings, p. 777.
[65] P. Montier-Garbet, these Proceedings, p. 92.
[66] P.C. Stangeby and J.D. Elder, J. Nucl. Mater. 220–222 (1995) 193.
[67] P.C. Stangeby and J.D. Elder, Nucl. Fusion 35 (1995) 1391.
[68] W.P. West et al., in: Proc. 21st EPS Conf. on Controlled Fusion and Plasma Physics, Vol. 18B, Part II (1994) p. 834.
[69] R.B. Campbell et al., J. Nucl. Mater. 196–198 (1992) 426.
[70] M. Nagami and JT-60 team, J. Nucl. Mater. 220–222 (1995) 3.
[71] P.C. Stangeby, J. Nucl. Mater. 176&177 (1990) 51.
[72] M. Shimada, Fusion Eng. Des. 15 (1992) 325.
[73] G.M. McCracken et al., in: Proc. 22nd EPS Conf. on Controlled Fusion and Plasma Physics, Vol. 19C, Part II (1995) p. 313.

[74] D. Jablonski, B. LaBombard, G.M. McCracken, S. Losgo, B. Lipschultz, I.H. Hutchinson, J. Terry and P.C. Stangeby, these Proceedings, p. 782.
[75] G.M. Staebler, J. Nucl. Mater. 220–222 (1995) 158.
[76] D. Post et al., J. Nucl. Mater. 220–222 (1995) 1014.
[77] A. Kallenbach et al., in: Proc. 22nd EPS Conf. on Controlled Fusion and Plasma Physics, Vol. 19C, Part II (1995) p. 5.
[78] G.F. Matthews et al., these Proceedings, p. 450.
[79] M.A. Mahdavi et al., Phys. Rev. Lett. 47 (1981) 1602.
[80] M.J. Schaffer et al., Nucl. Fusion 35 (1995) 1000.
[81] M.A. Mahdavi et al., J. Nucl. Mater. 220–222 (1995) 13.
[82] P.J. Harbour et al., in: Proc. of 22nd EPS Conf. on Controlled Fusion and Plasma Physics, Vol. 19C, Part IV (1995) p. 465.
[83] A. Kallenbach et al., Nucl. Fusion 35 (1995) 1231.
[84] H.-S. Bosch et al., Phys. Rev. Lett. 76 (1996) 2499.
[85] M.J. Schaffer, M.R. Wade, R. Maingi, P. Monier-Garbet, W.P. West, D.G. Whyte, R.D. Wood and M.A. Mahdavi, these Proceedings, p. 585.
[86] H.-S. Bosch et al., these Proceedings, p. 82.
[87] R.A. Hulse, Nucl. Technol. Fusion 3 (1983) 259.
[88] R. Dux et al., Plasma Phys. Control. Fusion 38 (1996) 989.
[89] N. Richard, B. Terrault, E. Haddad, J. Gunn, G. Abel, S. Chiu, J.-L. Gauvreau, H.H. Mai, W.W. Zuzak, these Proceedings, p. 760.
[90] D.P. Coster et al., these Proceedings, p. 690.
[91] H.-S. Bosch, private communication (1996).
[92] R. Simonini et al., in: Proc. of 21st EPS Conf. on Controlled Fusion and Plasma Physics, Vol. 18B, Part II (1994) p. 694.
[93] R. Stambaugh, 2nd Meet. of the ITER Divertor Physics and ITER Divertor Modelling and Database Expert Groups, Garching, Germany, 1995.
[94] G. Janeschitz, 3rd Meet. of the ITER Divertor Physics and ITER Divertor Modelling and Database Expert Groups, Naka, Japan, 1995.
[95] H.-S. Bosch et al., in: Proc. of 22nd EPS Conf. on Controlled Fusion and Plasma Physics, Vol. 19C, Part III (1995) p. 93.
[96] R. Schneider, H.S. Bosch, J. Neuhauser, D. Coster, K. Lackner and M. Kaufmann, these Proceedings, p. 701.
[97] P.C. Stangeby et al., Contrib. Plasma Phys. 34 (1994) 306.
[98] S. Tsuji et al., J. Nucl. Mater. 220–222 (1995) 400.
[99] K. Shimizu et al., J. Plasma Fusion Res. 71 (1995) 1227.